A Study of the Distribution of Sodium Cations in the Zeolites NaX, NaY and ZnNaY Using Carbon Monoxide Adsorption and ^{23}Na NMR Techniques

A. Seidel and B. Boddenberg

Lehrstuhl für Physikalische Chemie II, Universität Dortmund, Otto-Hahn-Str. 6, D-44227 Dortmund

Z. Naturforsch. **50a**, 199–210 (1995); received October 17, 1994

Herrn Professor Dr. Werner Müller-Warmuth zum 65. Geburtstag gewidmet

The zeolites NaX, NaY, Zn(55)NaY, and Zn(74)NaY were investigated by means of carbon monoxide adsorption and with static and magic angle spinning (MAS) ^{23}Na NMR spectroscopy. The Na^+ distribution between the sodalite (β)- and supercages of the fully hydrated zeolites NaX and NaY were found to agree with XRD results. In the hydrated zinc-exchanged zeolites the Na^+ ions almost exclusively populate the β-cages.

The adsorption isotherms of CO in the dehydrated zeolites were analyzed quantitatively to yield the concentrations of Na^+ residing in the supercages. The measured static and MAS ^{23}Na NMR spectra were analyzed by comparing their widths and shapes with simulated central transition patterns and yield, inter alia, the concentrations of Na^+ associated with the spectrum components. Arguments are put forward that ^{23}Na NMR of dehydrated zeolites is well suited to distinguish Na^+ cations in highly symmetric environments and mobile Na^+ species from others located on general positions, but further resolution is hardly feasible.

Key words: ^{23}Na NMR, Adsorption, Carbon monoxide, Zeolites, Zinc-exchange.

Introduction

In recent years, ^{23}Na NMR spectroscopy has repeatedly been applied to the study of the distribution of sodium cations in the sodium as well as partially ion exchanged forms of Faujasite type zeolites [1–11]. Since ^{23}Na is a spin $I = 3/2$ nucleus with large electric quadrupole moment, $eQ = 1.6 \cdot 10^{-48}$ Cm^2 [12], and since in the dehydrated state the cations are expected to be located on positions with different symmetries of the electric field gradient (EFG) tensor, the resulting spectra are difficult to analyze in terms of identification and quantitative determination of the various cation species.

In recent papers, we have studied the distribution of transition metal cations in partially exchanged zeolite NaY by means of ^{129}Xe and ^{13}C NMR spectroscopic and volumetric adsorption techniques using xenon atoms and carbon monoxide molecules as probes [13–22]. Since Xe and CO can only penetrate into the large voids (supercages) of Faujasites [13, 23], these methods, in contrast to ^{23}Na NMR spectroscopy, allow to differentiate between cations in various parts of the zeolitic void system. This aspect is of importance for the use of zeolites in catalysis and separation processes.

In the cited papers we were interested in the determination of the concentration and distribution of the transition metal cations but had treated only in a gross way the interaction of xenon and carbon monoxide with the residual sodium cations. The present contribution considers this aspect in more detail for partially zinc-exchanged zeolites NaY, and intends to correlate the results from this source of information with those coming from the analysis of the ^{23}Na NMR spectra.

Reprint requests to Prof. Dr. B. Boddenberg.

Experimental

The zinc-exchanged zeolites Zn(x)Y with $x = 55$ and 74% Na^+ replaced by Zn^{2+} cations were prepared by conventional ion exchange from zeolite NaY (Linde LZ-Y 52, Union Carbide, Si/Al = 2.4) with 0.1 mol dm^{-3} aqueous $Zn(NO_3)_2$ solution. Zeolite Zn(55)Y was prepared at ambient temperature, while repeated ion exchange at elevated temperature (80 °C) was necessary to obtain Zn(74)Y. The details of ion exchange and further pretreatment procedures as well as chemical and structural analysis of the materials

0932-0784 / 95 / 0200-0199 $ 06.00 © – Verlag der Zeitschrift für Naturforschung, D-72027 Tübingen

Table 1. Total cation concentrations of the investigated zinc-exchanged zeolites Y determined by chemical analysis (concentrations are in units of uc^{-1}).

Sample	Zinc content	Sodium content	Zn^{2+} for Na^+ exchange level (%)
Zn(55)Y	15.8	20.7	55
Zn(74)Y	21.0	10.6	74

have been described in [13]. Table 1 contains the overall concentrations of Zn^{2+} and residual Na^+ ions in the two zinc-exchanged zeolites used in this study. A further designation concerns the conditions under which ^{23}Na NMR spectra were recorded: Zn(x)YD which was dehydrated at rising temperature up to 400 °C, and Zn(x)YH which was fully hydrated over saturated aqueous NH_4Cl solution. Experiments were also performed on zeolites NaY(3.0) (Degussa, Si/Al = 3.0) and NaX (Linde 13X, Si/Al = 1.2), both under conditions designated D and H described before.

^{23}Na NMR spectra were measured with the aid of a solid state FT NMR spectrometer (Bruker MSL 400) operating at the resonance frequency $\omega_0/2\pi = 105.84$ MHz. The spectra obtained are represented on the commonly used shift scale with 1 mol dm^{-3} aqueous NaCl solution as external reference. All spectra were recorded with the zeolites placed in ZrO_2 rotors of 7 mm (rotation frequency $\nu_R = 5$ kHz) and 4 mm ($\nu_R = 10$ kHz) outer diameter in case of the hydrated and dehydrated samples, respectively. The dehydrated samples were prepared inside the rotors; a noticeable rehydration was not observed even after one week's exposure of the closed rotor to the laboratory atmosphere. Broad band excitation using $\pi/8$ pulses was always employed. The static spectra of the dehydrated samples were measured with the quadrupole echo two-pulse sequence. Depending on the sample under study, 10^3 to 10^5 time domain spectra with cycle delay times of, generally, 500 ms were accumulated before Fourier transformation.

Results

Figure 1 shows the adsorption isotherms at 298 K of carbon monoxide in the zeolites NaXD [24] and NaYD [25] as well as on the non-zinc sites of the zeolites Zn(x)YD (x = 55 and 74). The displayed data points of the latter zeolites were obtained by subtracting the amounts of CO adsorbed on zinc sites from the

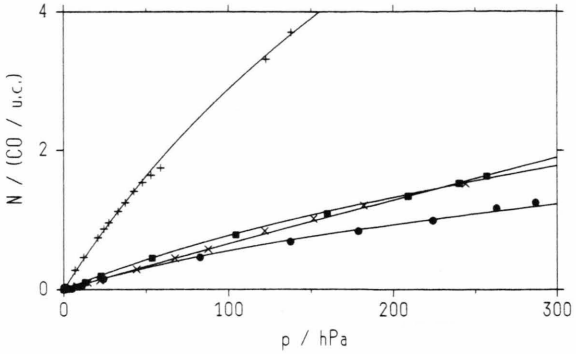

Fig. 1. Carbon monoxide adsorption isotherms (298 K) in the zeolites NaXD (+) and NaYD (×) as well as on the non-zinc sites in zeolites Zn(55)YD (■) and Zn(74)YD (●) [solid lines represent fittings according to the model discussed in the text].

experimental adsorption isotherm data at the corresponding equilibrium pressures [13]. These amounts can be calculated very faithfully from Langmuir adsorption equations fitting the initial parts of the experimental adsorption isotherms, whose steep rises up to pressures of about 10 hPa can overwhelmingly be attributed to the strong adsorption of CO on the zinc cation sites [13, 23].

The inspection of Fig. 1 reveals a much stronger adsorption of CO in zeolite NaXD than in NaYD, where a practically linear course of the adsorption isotherm is observed. The isotherms of the zinc-exchanged samples are close to NaYD but in contrast to the latter exhibit distinct curvature at higher pressures. Interestingly, the sample of higher zinc exchange exhibits the lower adsorption of CO.

Figure 2 shows the static (upper spectra) and MAS (lower spectra) ^{23}Na NMR spectra of the hydrated sodium and zinc-exchanged forms of the zeolites X and Y under study. The slightly asymmetric patterns of the zeolites NaY(3.0)H and NaYH under static conditions have peak maxima at − 1 ppm and halfwidths of about $\delta\nu = 0.7$ kHz. Under MAS, slight narrowing and more pronounced shape asymmetry are observed, which is indicative of a second sodium species resonating at about − 5 ppm. For zeolite NaXH the situation is similar to the former cases with, however, less well developed asymmetries. The static spectra of the zinc-exchanged samples are rather broad ($\delta\nu \approx 2$ kHz) and distinctly asymmetric. For Zn(55)YH the maximum appears at − 1 ppm and the shoulder at about − 5 ppm. At the higher zinc content these compo-

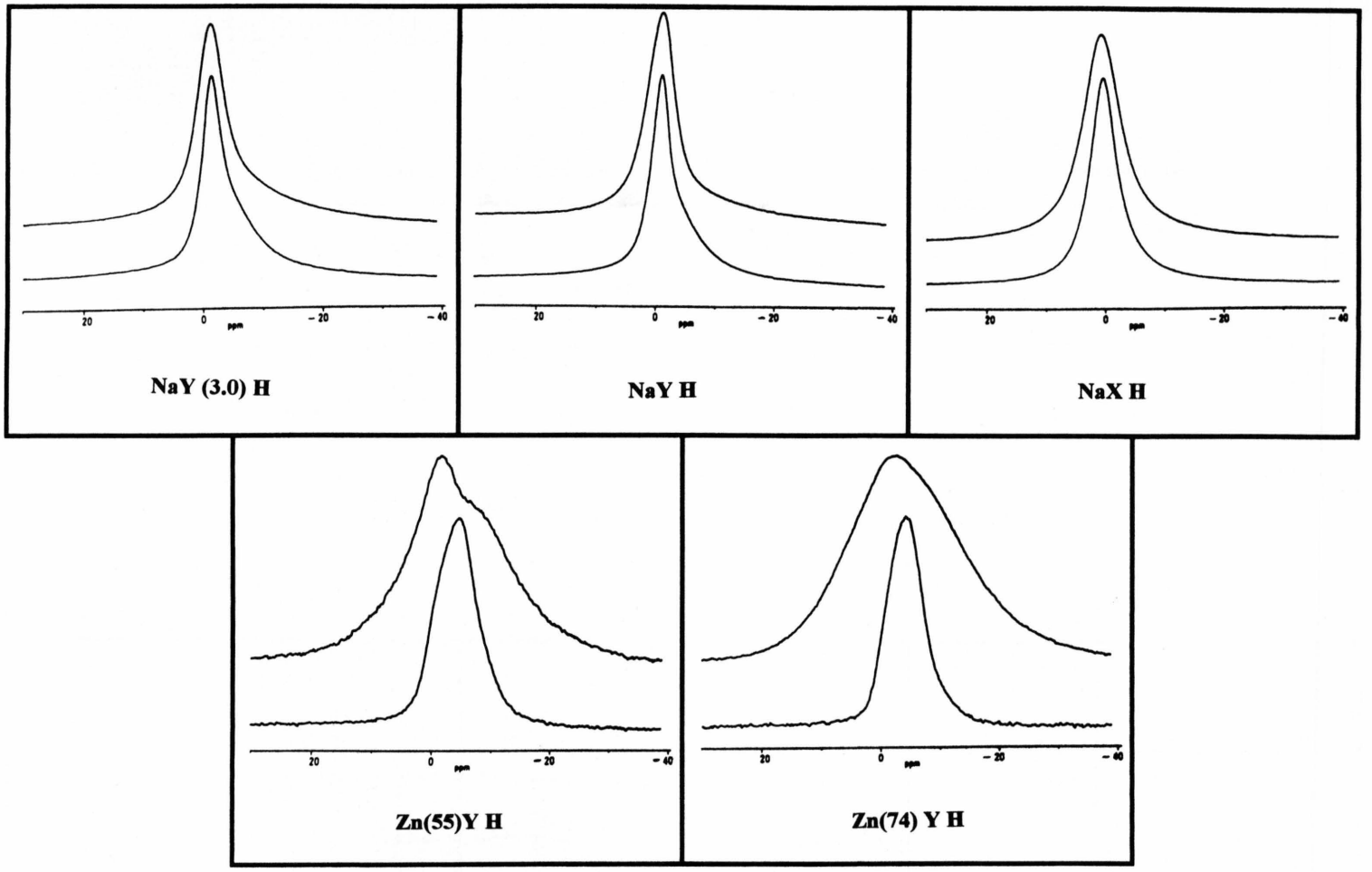

Fig. 2. Experimental ^{23}Na NMR spectra of hydrated zeolites recorded under static (upper spectra) and MAS conditions (lower spectra).

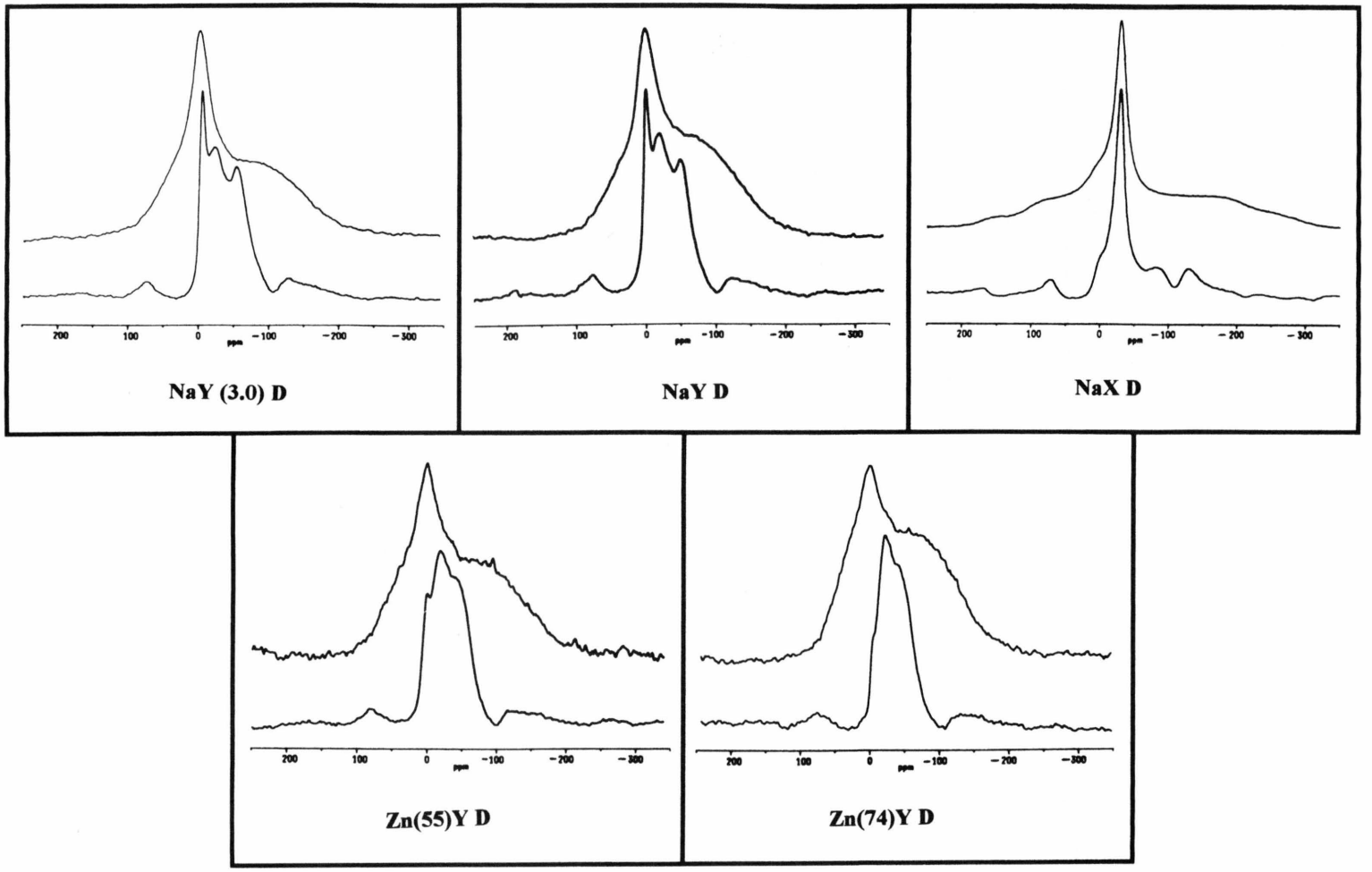

Fig. 3. Experimental ^{23}Na NMR spectra of dehydrated zeolites recorded under static (upper spectra) and MAS conditions (lower spectra).

nents obviously run together, leading to an unstructured line shape with maximum at − 3 ppm. Under MAS, for both zinc-exchanged samples the lines narrow considerably leading to slightly asymmetric line shapes with maxima at about − 5 ppm.

Figure 3 shows the static (upper spectra) and magic angle spinning (MAS) (lower spectra) ^{23}Na NMR patterns of the dehydrated sodium and zinc-exchanged forms of the Faujasites under study. The static spectra of each of the Y type zeolites are characterized by asymmetric shapes with well developed peaks in the vicinity of 0 ppm and broad humps with centers of gravity which are shifted upfield. The zeolite NaXD exhibits a well developed peak at about − 27 ppm on a broad base extending from about + 100 to − 200 ppm. The ^{23}Na MAS NMR spectra of the zeolites NaY show more resolved structure with mainly three peaks at − 4, − 23 and − 54 ppm, which for the zeolite NaX and the zinc-exchanged zeolites Y mostly degenerate into shoulders. The sharp low field line (− 4 ppm) of NaY is also seen in the zinc-exchanged samples, but with lower relative intensity, which moreover decreases with increasing zinc content.

Discussion

Adsorption of Carbon Monoxide

At ambient temperature, carbon monoxide molecules are known to penetrate only into the large voids (supercages) of dehydrated Faujasite type zeolites like the synthetic X and Y materials used in this investigation [13, 23]. In these cages, the concentration and distribution of sodium cations in the as-synthesized sodium zeolites is known from numerous X-ray and neutron diffraction studies (Table 2). So, in both NaX (Si/Al = 1.2) and NaY (Si/Al = 2.4) the 32 available crystallographic SII sites per unit cell (uc), which are at the six-rings connecting super- with sodalite(β)-cages, are practically fully occupied by Na^+ cations. The zeolite NaX contains further 8 supercage Na^+ ions per uc residing at the crystallographic SIII positions at the four-rings in front of the hexagonal prisms.

These findings about cation distribution and accessibility of the voids immediately suggest that the striking difference between the adsorption isotherms of CO in the zeolites NaXD and NaYD (Fig. 1) is associated with the occupation of SIII cation sites in the former material. It is an interesting observation that the initial heat of adsorption of CO in dehydrated NaX (32.6 kJ mol^{-1} [28]) is substantially larger than in NaY (23–25 kJ mol^{-1} [23, 29, 30]). This indicates a stronger adsorption of CO on Na^+ ions at SIII than at SII sites. This different behaviour may be considered caused by the circumstance that on SIII the cations are more freely exposed than on SII positions. Actually, the binding energy of a CO molecule to an isolated sodium cation is 40 kJ mol^{-1} according to quantum chemical calculations [31], which is in favour of this interpretation. Similar conclusions with respect to stronger bonding of CO and Xe to SIII cation sites have been drawn for the mono- and bivalent cations in silver [14–18], copper [19, 20], zinc [13], and cadmium [21, 22] exchanged zeolites Y.

The foregoing discussion suggests localized adsorption of CO on accessible sodium cations to be prevailing for both NaXD and NaYD. Because of the low concentration of the adsorbed molecules ($N \leq 0.5$ CO per supercage), lateral interaction can fairly be neglected so that the adsorption isotherms are expected

Table 2. Cation distributions in dehydrated zeolites (concentrations are in units of uc^{-1}).

Zeolith (Si/Al)	SI	SI′/SII′	SII	SIII	Method	Ref.
NaY (2.4)	7.7	19.5	30.3	–	XRD	[26]
NaY (2.4)	9.3	16.7	31.3	–	XRD	[26]
NaY (2.4)	7.1	18.7	32.3	–	neutron diffraction	[27]
NaY (2.4)	3	15	35	–	^{23}Na NMR	[5]
NaX (1.2)	3.8	32.3	30.8	7.9	XRD	[26]
Zn(55)Y (2.4)			1.5 Zn^{2+}	0.26 Zn^{2+}	CO adsorption	[13]
	0.6 Na^+	< 8 Na^+	15 ± 5 Na^+	1.7 ± 0.5 Na^+	CO adsorption/^{23}Na NMR	this work
Zn(74)Y (2.4)			2.2 Zn^{2+}	1.2 Zn^{2+}	CO adsorption	[13]
	0.1 Na^+	< 2 Na^+	8 ± 1 Na^+	1.4 ± 0.1 Na^+	CO adsorption/^{23}Na NMR	this work

to follow a Langmuir type equation of the form

$$N = \frac{n_1 k_1 p}{1 + k_1 p} + \frac{n_2 k_2 p}{1 + k_2 p}, \quad (1)$$

where N is the concentration of adsorbed CO at the equilibrium pressure p, and n_i, k_i $(i = 1, 2)$ are the concentrations and the CO adsorption constants of sites i, respectively. Here, $i = 1$ stands for the SII, and $i = 2$ for the SIII sodium cation sites. It is assumed that each site can accommodate just one CO molecule. In the case of NaYD the second term of (1) is missing ($n_2 = 0$ uc^{-1} according to Table 2). In the event that $k_i p \ll 1$, N is a linear function of p (Henry region) with

$$dN/dp = n_1 k_1 + n_2 k_2 . \quad (2)$$

Introducing in (1) and (2) the sodium concentrations $n_1 = 32$ uc^{-1}, $n_2 = 0$ uc^{-1} for zeolite NaYD and $n_1 = 31$ uc^{-1}, $n_2 = 8$ uc^{-1} for zeolite NaXD (Table 2), the adsorption constants can readily be evaluated from the initial slopes of the corresponding isotherms to be $k_1 = 2.1 \cdot 10^{-4}$ hPa^{-1} and $k_2 = 3.9 \cdot 10^{-3}$ hPa^{-1}. The solid curves in Fig. 1 represent the fitting curves obtained with these parameter data. The adsorption constants evaluated differ by more than one order of magnitude, reflecting the much stronger interaction strength of CO with Na^+ ions residing on the SIII positions. Both values of k_i are, however, much smaller than for the corresponding zinc sites (0.74 and 13 hPa^{-1}, [13]).

We turn now to the adsorption isotherms of CO on the sodium cation sites in the zinc-exchanged zeolites (Figure 1). If all the residual Na^+ ions in these zeolites (Table 1) were residing on SII positions, then the initial slopes of these isotherms would be lower than for NaYD, where these positions are fully occupied (Table 2). Since this is definitely not the case but, on the contrary, the initial slope of Zn(55)YD is even larger than for NaYD, we conclude that certain fractions of Na^+ ions reside on SIII positions. This conclusion is supported by the observation that the isotherms now exhibit distinct curvature. Inserting the previous adsorption constants k_1 and k_2 into (1), the concentrations n_1 and n_2 can be obtained with the aid of a fitting procedure. Nice fits (solid curves in Fig. 1) are obtained with the values for n_1 and n_2 that are collected in Table 2. A comparison of these figures with the total residual concentrations of sodium cations in these zeolites (Table 1) leads to the conclusion that through the zinc exchange the small cavities have been depleted almost completely of Na^+ species.

We wish to emphasize that the values of the adsorption constants k_1 and k_2 evaluated from the CO adsorption isotherms of NaXD and NaYD and, as a consequence, also of the sodium cation concentrations n_1 and n_2 of the zinc-exchanged samples rely on the XRD results reported for the former zeolites. The main question concerns the nature and location of the ca. six Na^+ cations per unit cell which in the case of zeolite NaXD are not detected by the XRD technique. Actually, we have tacitly assumed that these surplus cations do not provide adsorption centers for CO. Below we shall develope arguments that the sodium cations under question still carry residual water molecules. In this event the surplus cations residing in the supercages are readily imaginable to lose the capability of acting as adsorption sites for CO. If by some further work the aforementioned assumption should turn out to be erroneous, a reevaluation of the adsorption constants and of the sodium concentrations of the zinc-exchanged zeolites would be required. We have verified that the measured adsorption isotherms of CO in NaXD and the zinc-exchanged samples can also approximately be reproduced even if each of the surplus cations provides strong adsorption centers for CO.

^{23}Na *NMR of Hydrated Zeolites*

Hydrated Faujasite type zeolites have repeatedly been investigated by means of ^{23}Na NMR spectroscopy, mainly under magic angle spinning (MAS) conditions [1–3, 9–11]. Except under special preparation conditions [2] the measured spectra could be decomposed into two signal components with chemical shifts of about -5 and -1 ppm (related to our aqueous NaCl solution reference) which are assigned to sodium cations residing in the sodalite (β)- and supercages, respectively. Guided by this experience, we were also able to resolve each of the measured spectra into such two components of Gaussian lineshape under both static and MAS conditions. Three typical examples are shown in Figure 4a–c. The fitting parameters, namely the isotropic chemical shifts δ_{iso}, the widths at half height $\delta\nu$, and the relative intensities I_{rel} of the complete set of experimental spectra are collected in Table 3. The last column of this table contains the Na^+ concentrations calculated from the averages of I_{rel} from the static and MAS measurements on the basis of the nominal overall Na^+ content (zeolites NaY and NaX) and of the Na^+ concentration data

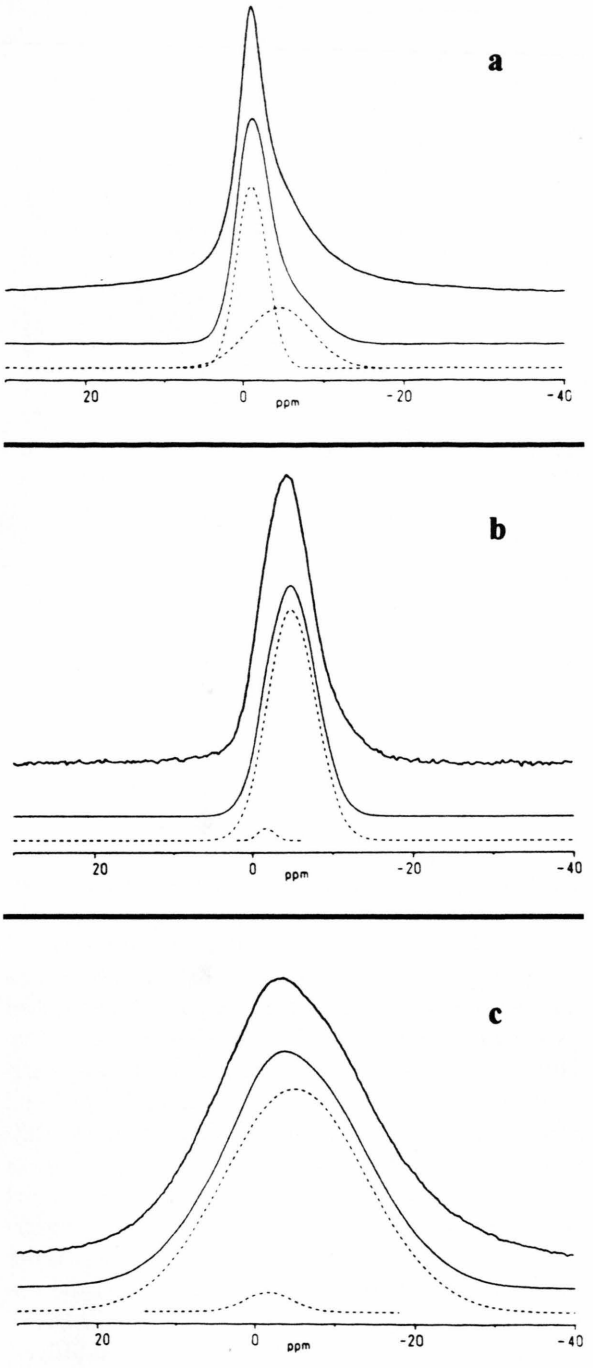

Fig. 4. Comparison of experimental (upper spectra) and simulated (lower spectra) ^{23}Na NMR spectra of hydrated zeolites; the decomposition of the spectra is shown by dotted lines [a) NaYH/MAS; b) Zn(74)YH/MAS; c) Zn(74)YH/broad line].

Table 3. Data obtained from the analysis of the MAS and static ^{23}Na NMR spectra of hydrated zeolites.

Zeolite (Si/Al)	δ_{iso} / ppm	$\delta\nu^{MAS}$ / kHz	$\delta\nu^{STA}$ / kHz	I_{rel}^{MAS} (I_{rel}^{STA})	n_{Na^+} / uc^{-1}
NaY (3.0)	−1.5	0.47	0.67	53 (54)	25
	−5.0	1.00	1.74	47 (46)	23
NaY (2.4)	−1.1	0.47	0.67	59 (69)	36
	−4.5	1.00	1.74	41 (31)	20
NaX (1.2)	0.3	0.52	0.75	73 (71)	62
	−3.0	1.12	1.74	27 (29)	24
Zn(55)Y (2.4)	−1.5	0.25	0.50	4 (7)	1
	−5.0	0.75	2.12	96 (93)	20
Zn(74)Y (2.4)	−1.7	0.25	0.75	2 (3)	0.3
	−5.0	0.75	2.24	98 (97)	10.3

listed in Table 1 (zinc-exchanged zeolites). We wish to emphasize that the line positions, i.e. the isotropic chemical shifts δ_{iso}, come out to be the same within experimental error (± 0.2 ppm) under both measuring conditions.

Considering the last column of Table 3, it may be realized that the β-cage Na^+ concentrations are virtually the same for each of the sodium zeolites under study, i.e. they are independent of the Si/Al ratio. The concentrations of sodium cations within the supercages obtained in this study increase from 36 uc^{-1} in case of sample NaYH up to 62 uc^{-1} in case of NaXH. These values are in good agreement with the values of 29–42 uc^{-1} and 50–61 uc^{-1} obtained for the respective zeolites by means of XRD techniques, if sodium cations which cannot be detected are assumed to reside unlocalized in the supercages [26]. The zinc-exchanged zeolite Zn(55)YH also exhibits a concentration of 20 Na^+ cations within the β-cages of one unit cell, whereas its supercages are almost completely bereft of such ions. Interestingly, the charge of the depleted sodium cations (ca. 35 e/uc) formally corresponds to the charge of the zinc cations introduced ($2 \cdot 16$ e/uc = 32 e/uc, Table 1). So, under the view of charge balance the zinc cations can be assumed to reside practically exclusively in the supercages. The lack of zinc cation exchange into the β-cages can readily be explained by the large diameter of the Zn^{2+} cation's hydration shell which prevents the transition of the cations through the bordering six-membered windows.

In the zeolite Zn(74)YH the residual sodium cations are also almost exclusively contained in the β-cages with concentration of about one half the value that in

the preceding section has been considered to achieve the charge balance. Although we do not have any direct evidence, we may assume that charge balance is still maintained by about 5 additional Zn^{2+} cations also residing in the β-cages. The kinetic requirement of zinc cation penetration through the six-ring windows between the sodalite- and supercages can be considered to be met by the high temperature (80 °C) applied during the ion exchange procedure. Probably, a partial instantaneous desolvation of the zinc cations at the openings accounts for the intercage exchange.

Table 3 contains a couple of further interesting details which are worth considering, but are postponed to a forthcoming paper with new experimental material added. In this paper the systematic behaviour of the chemical shifts as functions of the Si/Al ratio and the influence of the zinc-exchange on the linewidths under both static and MAS conditions will be analyzed in terms of structural and dynamical aspects.

^{23}Na NMR of Dehydrated Zeolites

With the aid of the versatile NMR techniques presently available, such as magic angle spinning (MAS), double rotation (DOR) and two-dimensional nutation spectroscopies, much work has been devoted to assess the sitings and concentrations of sodium cations in the framework of dehydrated Faujasite type zeolites [3–8]. In [5] it has been claimed that by simulation of the shapes of the complex MAS spectra obtained for a dehydrated zeolite NaY at different Zeeman field strengths up to 17.6 T, as many as four different sodium cation species can be identified and their concentrations determined.

Following the lines of theoretical analysis of MAS spectra presented in [4, 32–33], we have simulated the central transition isotropic MAS patterns of the zeolites NaYD and NaY(3.0)D on the basis of a two-site model using a home-written computer program. In Fig. 5a we show for NaYD the comparison of the experimental result with the simulated pattern consisting of a narrow quadrupole pattern appearing as a Gaussian-like singlet at − 4 ppm and a second order quadrupole powder pattern which accounts for the two maxima at − 23 and − 54 ppm. The complete set of parameters used for the spectra simulation of this zeolite as well as for NaY(3.0)D, namely the isotropic chemical shifts δ_{iso}, the quadrupole coupling constants QCC, and the asymmetry parameters η characteristic for the electric field gradient (EFG) at the sodium nuclear sites and, finally, the experimental and rescaled [34] relative intensities, I_{rel} and I, are collected in Table 4. The EFG parameters used to simulate the line at − 4 ppm are the result of a ^{23}Na DOR NMR study published in [5]. A convolution with Gaussians of halfwidth $\delta\nu$ (Table 4) was always performed in order to account for residual line broadenings. Obviously, a good fit of the experimentally determined MAS patterns can be achieved. The obtained parameter data compare very well with those coming from MAS pattern simulations published in [4]. We notice the surprisingly large values of the individual linewidths $\delta\nu$ under the employed MAS conditions. In the light of the recent high field study [5] the applied two-site model may appear somewhat oversimplified. However, in a later section we shall put forward arguments indicating that further resolution of the second order quadrupole component appears to be an artificial procedure. Following closely the suggestions of other authors [3, 4], we associate the narrow singlet with sodium cations on the SI positions in the centers of the hexagonal prisms, and the second order quadrupole component with Na^+ cations at the six-ring windows of the supercage SII and the β-cage SI′ positions. With this assignment we obtain an SI Na^+ concentration of about 1–2 cations per unit cell in case of NaYD, which is distinctly less than is found by XRD measurements (Table 2), but aggrees rather well with the NMR results of other authors [4, 5].

The most prominent line at − 27 ppm of zeolite NaXD, which has no counterpart in the NaY zeolite

Table 4. Parameter data used for the simulation of MAS and static ^{23}Na NMR spectra of dehydrated zeolites (* data taken from [5]).

Zeolite (Si/Al)	δ_{iso} ppm	QCC MHz	η	$\delta\nu^{MAS}$ kHz	$\delta\nu^{STA}$ kHz	I_{rel}^{MAS} (%)	I^{MAS} (%)
NaY	−4	0.1*	0*	1.0	3.5	16	2
(3.0)	3	4.3	0.3	1.4	7.0	84	98
NaY	−4	0.1*	0*	1.0	3.5	16	2
(2.4)	3	4.3	0.3	1.4	7.0	84	98
NaX	0	0.1*	0*	2.5	4.0	14	2
(1.2)	−27	0	–	2.0	3.0	42	2
	5	5.2	0.1	2.8	7.0	44	96
Zn(55)Y	−2	0.1*	0*	1.25	3.5	11	3
(2.4)	−31	0	–	2.0	4.0	6	<1
	3	4.0	0.3	1.4	7.0	83	97
Zn(74)Y	3	0.1*	0*	1.0	3.3	4	1
(2.4)	−22	0	–	2.5	5.0	8	1
	4	3.8	0.4	1.4	7.0	88	98

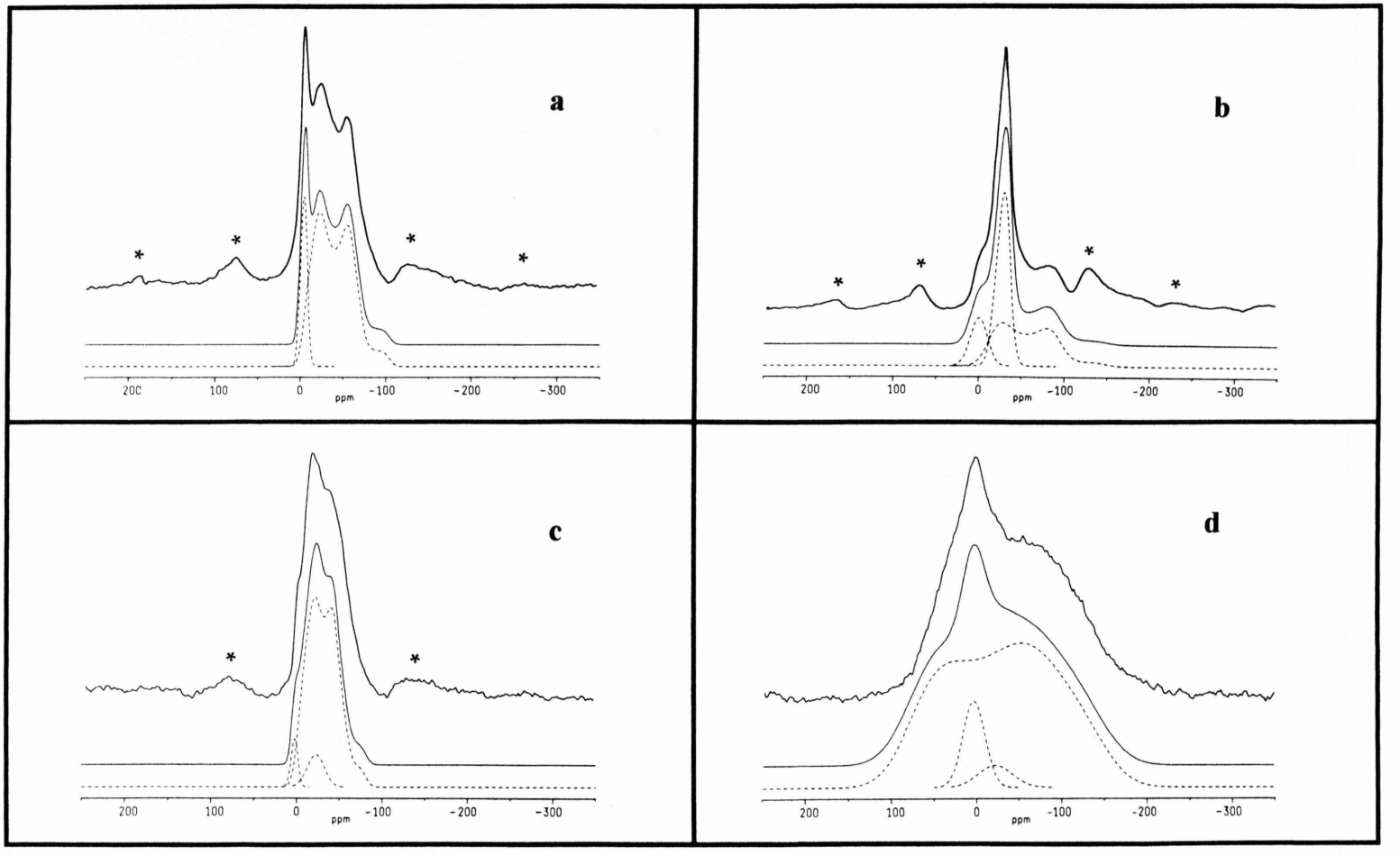

Fig. 5. Comparison of experimental (upper spectra) and simulated (lower spectra) ^{23}Na NMR spectra of dehydrated zeolites; the decomposition of the patterns is shown by dotted lines; asterisks denote rotational side bands in the experimental MAS spectra [a) NaYD/MAS; b) NaXD/MAS; c) Zn(74)YD/MAS; d) Zn(74)YD/broad line].

case, is considered to result from isotropic motional averaging and so is ascribed to mobile Na^+ cations. This conclusion is substantiated by the observation that this line appears at the same position in the static as well as in the MAS spectrum and exhibits similar shape and width in both cases. Actually, it is hardly conceivable that besides the SI positions further sites of approximately cubic symmetry are available in the zeolite framwork which might account for a such narrow static line. As this signal is not observed in the NaYD case, we associate it with the non-localized cations escaping detection by the XRD-method [26]. The required motional averaging is considered to result from complexation of these cations with residual water molecules which under the applied dehydration procedure have not been removed. Interestingly, zeolite samples carrying intentionally introduced small amounts of water [5] exhibit also narrow upfield shifted ^{23}Na MAS NMR lines. The slight shoulder at about 0 ppm observed in the experimental MAS pattern of NaXD is considered to come from Na^+ ions on SI positions which are less frequent in NaXD than in NaYD both on an absolute and a relative scale according to XRD results (Table 2). Besides these features, a second order quadrupole pattern of similar type as in NaYD can be seen.

Guided by these qualitative considerations, a simulation of the MAS pattern of NaXD was performed with three cation species, of which two are characterized by singlets at 0 and -27 ppm and the other one by a second order quadrupole pattern. Again, the singlet at 0 ppm was represented by a narrow quadrupole pattern with the same EFG parameters as in the previous NaY case. In Fig. 5b the simulated pattern with its constituent components is compared with experiment. A reasonable agreement is achieved with the fitting parameters collected in Table 4. It is observed that the parameters describing the second order quadrupole component are different from the corresponding values obtained for the zeolite NaYD. This is especially true for the MAS linewidth $\delta\nu$ which in the case of NaXD is distinctly larger.

We now turn to the discussion of the ^{23}Na NMR spectra of the partially zinc-exchanged zeolites Zn(55)YD and Zn(74)YD. Referring to the previous discussions the qualitative picture is straightforward: like for the parent zeolite NaYD there is a Gaussian-like line at about 0 ppm that decreases with increasing zinc content, and a second order quadrupole pattern which is now superimposed by a small isotropic component at -31 and -22 ppm for zeolites Zn(55)YD and Zn(74)YD, respectively. As an example, we show the simulated MAS pattern for Zn(74)YD in Figure 5c. It is seen to reproduce the experimental result very well. The parameter values used for the simulation of the MAS patterns of both zinc-exchanged zeolites are collected in Table 4.

Simulations of each of the static patterns displayed in Fig. 3 were carried out by calculating the central transition second order quadrupole coupling powder line shapes with the respective EFG parameters obtained from the MAS pattern simulations (Table 4) [33, 35]. Isotropic shielding tensors were assumed (δ_{iso} from Table 4) and the dipolar couplings were taken account of by convolution with Gaussian lines. As an example, we show in Fig. 5d the obtained result for zeolite Zn(74)YD. Although the general features of experiment are reproduced, major deviations with respect to line shape are recognized. These discrepancies are most probably due to the anisotropy of the magnetic shielding coupling arising not only from the electron cloud of the sodium cations themselves but also from the induced moments of the nearby atoms, especially the next-nearest neighbour oxygens. For instance, the shielding anisotropies due to framework atoms and nearby cations at Li^+ positions in the six-ring windows of zeolites type A, X, and Y are in the range of $\Delta\sigma = -20$ to -25 ppm [36, 37]. Although the positions of the sodium cations are somewhat different [26, 27] from those of Li^+, this shielding anisotropy effect can substantially contribute to the spectrum distortions observed.

A critical examination of the analysis of the experimentally determined ^{23}Na NMR static and MAS patterns by the line shape comparison method applied in this work and by other authors [3–5] seems to be in order. If it were known that the second order quadrupole pattern is generated by sodium cations residing on equivalent sites, then the line shape analysis in terms of the electric field gradient parameters (QCC and η) should be a reliable method for the determination of relative intensities, and therefore of relative Na^+ cation concentrations. If, however, already two inequivalent sodium species are present which give rise to second order patterns with somewhat different EFG parameters, a multi-parameter fit has to be accomplished for the extraction of reliable sodium site concentrations. This fit, in general, is not appropriate to lead to a unique result. Seemingly, a way out of this dilemma is the study of the Zeeman field dependence

of the MAS patterns, as has been proposed in [5]. The basic problem, however, lies in the long known circumstance that the EFG parameters at a sodium site are strongly dependent on the nearby Si,Al configuration and, most important, on the configuration of the surrounding occupied cation sites [38–40]. This entails that a large number of Si/Al/Na-configurations, each resulting in different EFG parameters, will lead to a spectrum of superimposed lineshapes that cannot be resolved. The experiments performed in this work show that this superposition leads to a broad component within the MAS spectrum which is very similar to a second order quadrupole powder pattern of a single nuclear species exhibiting, however, large line broadening $\delta\nu$. So, the EFG parameters extracted from lineshape simulations seem to represent some mean values of components which, moreover, appear with differently scaled intensities [34]. These considerations suggest that the determination of relative concentrations of sodium cations is questionable. On the other hand, the extreme sensitivity of the method towards Na^+ cations in highly symmetric environments and in the state of high mobility is appreciated.

Conclusions

^{23}Na NMR techniques have been used to study the distribution and relative concentrations of sodium cations in hydrated and dehydrated Faujasite type zeolites comprising the as-synthesized sodium forms of the X and Y type as well as partially zinc-exchanged Y type samples. In the hydrated state, the distribution of the Na^+ ions between the sodalite- and supercages can well be assessed and the influence of exchanged zinc-cations on this distribution is quantified. In the dehydrated state, the presence of sodium cations in highly symmetric environments and of mobile species (in NaX) at very low concentration levels can easily be observed. Sodium cation species located in less symmetric positions within the alumo-silicate framework yield overlapping second order quadrupole patterns that withstand decomposition into components attributable to sodium cations residing on different crystallographic sites. So, by means of ^{23}Na MAS NMR spectroscopy we do not recognize any way to reliably distinguish among sodium cations on non-cubic sites such as SII and SIII in the supercages as well as SI′ and SII′ in the β-cages.

The adsorption part of the present study shows that carbon monoxide interacts sufficiently strongly and selectively with sodium cations. So, by this technique the cations in the supercages are detected, and here the cations residing on SII positions can be distinguished from others, presumably occupying SIII sites.

Acknowledgements

We thank Mrs. Sonja Franke for permission to use the carbon monoxide adsorption isotherm data of zeolite NaXD.

[1] L. B. Welsh and S. L. Lambert, in Perspectives in Molecular Sieve Science, edited by W. H. Flank and T. E. White, ACS Symposium Series Vol. **368,** Washington, D.C. 1988, p. 33.
[2] H. K. Beyer, G. Pal-Borbely, and H. G. Karge, Microporous Materials **1,** 67 (1993).
[3] M. Hunger, G. Engelhardt, and J. Weitkamp, in Zeolites and Related Microporous Materials: State of the Art 1994, edited by J. Weitkamp, H. G. Karge, H. Pfeifer, and W. Hölderich, Elsevier, Amsterdam 1994, Studies in Surface Science and Catalysis Vol. **84,** p. 725.
[4] M. Hunger, G. Engelhardt, K. Koller, and J. Weitkamp, Solid State Nuclear Magnetic Resonance **2,** 111 (1993).
[5] G. Engelhardt, M. Hunger, H. Koller, and J. Weitkamp, in Zeolites and Related Microporous Materials: State of the Art 1994, edited by J. Weitkamp, H. G. Karge, H. Pfeifer, and W. Hölderich, Elsevier, Amsterdam 1994, Studies in Surface Science and Catalysis Vol. **84,** p. 421.
[6] R. Jelinek, S. Özkar, H. O. Pastore, A. Malek, and G. A. Ozin, J. Amer. Chem. Soc. **115,** 563 (1993).
[7] R. Jelinek, S. Özkar, and G. A. Ozin, J. Amer. Chem. Soc. **114,** 4907 (1992).
[8] H. A. M. Verhulst, W. J. J. Welters, G. Vorbeck, L. J. M. van de Ven, V. H. J. De Beer, R. A. van Santen, and J. W. de Haan, J. Chem. Soc., Chem. Commun. 639 (1994); J. Phys. Chem. **98,** 7056 (1994).
[9] R. Challoner and R. K. Harris, Zeolites **11,** 265 (1991).
[10] K.-J. Chao, S. H. Chen, and S. B. Liu, Stud. Surf. Sci. Catal. **60,** 123 (1991).
[11] K.-J. Chao and Ch.-F. Lin, Collect. Czech. Chem. Commun. **57,** 710 (1992).
[12] R. K. Harris, Nuclear Magnetic Resonance Spectroscopy, A Physicochemical View, Longman, Avon 1986, p. 238.
[13] B. Boddenberg and A. Seidel, J. Chem. Soc. Faraday Trans. **90,** 1345 (1994).
[14] R. Burmeister, R. Große, B. Boddenberg, A. Gedeon, and J. Fraissard, J. Phys. Chem. **95,** 2443 (1991).
[15] A. Gedeon, R. Burmeister, R. Große, B. Boddenberg, and J. Fraissard, Chem. Phys. Lett. **179,** 191 (1991).
[16] R. Große, A. Gedeon, J. Watermann, J. Fraissard, and B. Boddenberg, Zeolites **12,** 909 (1992).
[17] B. Boddenberg and J. Watermann, Chem. Phys. Lett. **203,** 531 (1993).

[18] J. Watermann and B. Boddenberg, Zeolites **13,** 427 (1993).
[19] B. Boddenberg and M. Hartmann, Chem. Phys. Lett. **203,** 243 (1993).
[20] M. Hartmann and B. Boddenberg, Microporous Materials **2,** 127 (1994).
[21] B. Boddenberg and T. Sprang, J. Chem. Soc. Faraday Trans. **91,** 163 (1995).
[22] T. Sprang and B. Boddenberg, J. Chem. Soc. Faraday Trans., in press.
[23] T. A. Egerton and F. S. Stone, J. Chem. Soc., Faraday Trans. I **69,** 22 (1973).
[24] S. Franke, Ph.D. Thesis, Universität Dortmund 1995.
[25] M. Hartmann, Ph.D. Thesis, Universität Dortmund 1993.
[26] W. J. Mortier, Compilation of Extra Framework Sites in Zeolites, Butterworth, Guildford 1982, and references cited therein.
[27] A. N. Fitch, H. Jobic, and A. Renouprez, J. Phys. Chem. **90,** 1311 (1986).
[28] J. Haber, J. Ptaszynski, and J. Sloczynski, Bull. Acad. Pol. Sci., Ser. Sci. Chim. **23,** 709 (1975).
[29] T. A. Egerton and F. S. Stone, J. Colloid Interface Sci. **38,** 195 (1972).
[30] T. A. Egerton and F. S. Stone, Trans. Faraday Soc. **66,** 2364 (1970).
[31] D. A. Dixon, J. L. Gole, and A. Komornicki, J. Phys. Chem. **92,** 1378 (1988).
[32] D. Müller, Ann. Phys. **39,** 451 (1982).
[33] A. I. Popov and K. Hallenga (Eds.), Modern NMR Techniques and their Application in Chemistry, Practical Spectroscopy Series Vol. **11,** Marcel Dekker, New York 1991.
[34] D. Massiot, C. Bessada, J. P. Coutures, and F. Taulelle, J. Magn. Reson. **90,** 231 (1990).
[35] K. Narita, J.-I. Umeda, and H. Kusumoto, J. Chem. Phys. **44,** 2719 (1966).
[36] B. Schimiczek, R. Greth, and B. Boddenberg, Molec. Phys. **82,** 369 (1994).
[37] H. Schwarz, R. Greth, and B. Boddenberg, unpublished results.
[38] H. Lechert and H. W. Henneke, in Molecular Sieves II, edited by J. R. Katzer, ACS Symposium Series Vol. **40,** Washington, D.C. (1977), p. 53.
[39] H. Lechert, Ber. Bunsenges. Phys. Chem. **77,** 697 (1973).
[40] H. Lechert, W. Gunsser, and A. Knappwost, Ber. Bunsenges. Phys. Chem. **72,** 84 (1968).